RSC Advances

ROYAL SOCIETY OF CHEMISTRY

www.rsc.org/advances

Facile synthesis CNTs@Fe@SiO_2 ternary composite with enhanced microwave absorption performance

Hualiang Lv[a], Guangbin Ji [a], Haiqian Zhang[a], Youwei Du[b]

Received (in XXX, XXX) Xth XXXXXXXXX 200X, Accepted Xth XXXXXXXXX 200X
DOI: 10.1039/b000000x

Magnetic/dielectric core-shell structure has been regarded as an ideal high-performance electromagnetic absorption material due to its novel multiple-loss mechanism. However, the poor impedance matching property of dielectric shell may lead to the high reflection of electromagnetic wave from the interface of shell. Thus, we ingeniously use the magnetic material as the shells while the dielectric material as the core. Such a change not only decreases the electromagnetic wave reflection, but also causes the strong interface polarization. Subsequently, the wave-transparent material of SiO_2 was further coated on the surface of magnetic shell which was not only protected it out of oxidation but also increased the impedance matching performance. Based on the above design, in this study, we fabricated the CNTs@Fe@SiO_2 ternary core-structure using a simple two-step approach consisting a pyrosis and decomposition process. As compared with the pure CNTs and CNTs@Fe, the obtained CNTs@Fe@SiO_2 composite shows the obviously enhanced electromagnetic absorption properties. In particular at a thin thickness of 1.5 mm, the optimal reflection loss value is as high as -14.2 dB which is better than most of the reported CNTs based absorbers. The improved electromagnetic absorption property can be attributed to the perfect impedance matching behavior and the multiple interface polarization effect.

1. Introduction

In recent years, core-shell structure has aroused extensive attention due to its potential application in sensor, catalysis, and lithium battery field.[1-2] Currently, great efforts demonstrated that the composite with core-shell structure is suitable for the electromagnetic absorption absorber.[3-4] Generally, the electromagnetic absorber is a kind of functional material which can let the incidence electromagnetic wave incidence into the absorber and then attenuate it into thermal energy.[5-6] Depending on the attenuation way, we may classify the electromagnetic absorber into two parts, one is magnetic loss materials, liking Fe, Co, Ni, ferrite, while the other is the dielectric loss material including graphene, SiC, ZnO, CuS and so on.[7-8] The dielectric/magnetic core-shell composites have two big advantages in electromagnetic absorption field. On the one hand, the sample presents the high chemical stability owing to the dielectric shell. On the other hand, the attenuation way is multiples as compared with single magnetic materials or dielectric loss.[9-10] As a result; these kinds of absorbers exhibit the obviously enhanced electromagnetic absorption properties. For example, both Fe_3O_4 and SnO_2 showed a poor electromagnetic absorption property which the optimal reflection loss values were less than -10 dB. Whereas the minimum reflection loss value of Fe_3O_4@SnO_2 increased to -36.5 dB.[11] Similar result also be observed in other absorbers including Fe_3O_4 based core-shell structures, such as Fe_3O_4@TiO_2,[12-13] Fe_3O_4@ZnO,[14] Fe_3O_4@C[15] and the Ni based composites *e.g*: Ni@Al_2O_3,[16] Ni@ZnS,[17] Ni@ZnO[18] or FeCo@C,[19] and Co@ZnO[20]. Unfortunately, the optimal RL_{min} values of these magnetic@dielectric composites hardly locate at a thin thickness (<2 mm) due to the poor impedance matching properties under high frequency. That is the main drawback in magnetic@dielectric materials which can be explained by the impedance matching theory:[21-23]

$$Z=Z_1/Z_o \quad (1)$$
$$Z_1=(\mu_r/\varepsilon_r)^{1/2} Z_o \quad (2)$$
$$\mu_r=\mu'-j\mu'' \quad (3)$$
$$\varepsilon_r=\varepsilon'-j\varepsilon'' \quad (4)$$
$$|\varepsilon|=(\varepsilon'^2+\varepsilon''^2)^{1/2} \quad (5)$$
$$|\mu|=(\mu'^2+\mu''^2)^{1/2} \quad (6)$$

Where Z_1 is stand for the impedance matching value of the absorbent, Z_0 is the free space of impedance matching. ε_r and μ_r are the complex permittivity and permeability value, respectively. From the equations, we can conclude that the poor impedance matching ratio results from a big ε_r and small μ_r. Meanwhile, equation (5) also indicates that the larger ε_r (or μ_r) value is related to the big ε' and ε'' (or μ' and μ'' value). For most of non-magnetic dielectric material, the ε' and ε'' value are so large while the μ_r is equal to 1 (for nono-magnetic material, the μ' is equal to 1 and the μ'' is close to 0 which make the μ_r approach to 1). Such an unmatched ε_r and μ_r value may led to the poor impedance matching properties. For instance, the ε' value of carbon is about 40-100 and the ε'' value is ranged in 10-50.[24] That is the main reason why the dielectric loss materials hardly obtain an excellent electromagnetic absorption properties. Thus, the dielectric material is not suitable for the shell. Different from the dielectric materials, the magnetic materials exhibit obvious advantage over the impedance matching properties. In fact, a higher saturation magnetization value (*Ms*) for magnetic material is always attributed to the higher μ' value based on the following equation: [25-26]

$$(\mu_0-1) f_o=(1/3\pi)M_s \quad (7)$$

More importantly, the high *Ms* value is better for magnetic loss ability which results in the increase of μ'.

In this study, we introduce a new type of dielectric/magnetic core-shell absorber which the CNTs served as the core and Fe nano-particles originated from a $Fe(CO)_5$ decomposition process as the shell (see Fig. 1). It is not difficult to understand that Fe shows a higher *Ms* value (220 emu/g) than most of other magnetic materials, liking Co (180 emu/g), Ni (55 emu/g) and Fe_3O_4 (100 emu/g) , ferrite (less than 100 emu/g).[27] As a classic carbon material, CNTs possess the better dielectric ability than carbon material (*i.e.*: graphene, carbon sphere, *etc*.) or other dielectric materials.[28] The relatively lower density of CNTs is also considered to be a big advantage as the light-weight absorber. What's more, the as-prepared CNTs@Fe is further coated by the SiO_2 to avoid the possible Fe oxidation process. It should be pointed out that the pure SiO_2 has no obvious electromagnetic absorption; however, its excellent transmissivity and high impedance matching make it more suitable for the novel magnetic/dielectric absorbing composites. Such kind of ternary core-shell structure is apt to reach an excellent electromagnetic absorption property at a thin coating thickness, which greatly satisfy the demand of light-weight.

2. Experimental section

2.1 Materials

Tetraethoxysilane (TEOS, $Si(OC_2H_5)_4$, 95 wt%), ammonium (NH_4OH, 28%) and methanol were purchased from the Sinopharm Chemical Reagent Co. Iron Pentacarbonyl ($Fe(CO)_5$) was purchased from the Beijing XinDingTengFei Co. Kerosene was purchased from Chengdu ChengTai Co. The CNTs used in this study was purchased from Shenzhen Nano Technical Co with 10-20 μm in length, 10-15 nm in inter diameter, and ~40-50 nm external diameter. All of the chemical regents used in this reagents are analytically pure and without further purification.

2.2 Preparation of CNTs@Fe core-shell structure

The Fe coating layer was prepared by a heated-decomposed process. In detail, 400 mg of CNTs was dissolved into a four-flask which containing 500 mL kerosene and then ultrasonic treatment 1 h to ensure the CNTs dispersed well. Afterward, the flask was heat at 200 ^oC for 6 h. During the pyrolysis process, the four-flask was connected with reflux unit, mechanical agitator and flow tube, temperature controller. Actually, $Fe(CO)_5$ was not added into the four-flask at the early stage. Owing to the N_2 steam and relatively high temperature (60 ^oC), $Fe(CO)_5$ will flow into the four-flask. The speed of $Fe(CO)_5$ can be controlled by the flow rate of N_2 (10 mL/min). After the temperature cooled to room temperature, the CNTs@Fe was obtained by the magnetic separation and washed 5 times by ethanol. The generation of iron coating layer was under the following chemical equation:[29]

$$Fe(CO)_5 = Fe + 5CO \quad (8)$$

2.3 Preparation of CNTs@Fe@SiO_2 ternary composite

Silica oxide coating of CNTs@Fe was produced via a modified Stober method.[30-31] Typical, 200 mg of the CNTs@Fe was dispersed in a mixture of 80 mL distilled water, 20 mL absolute ethanol and 2 mL ammonium. Next, every 30 (totally 4 mL) min, 0.5 mL TEOS was dropped into the mixed solution. After 8 h mechanical stirring, the finally sample was collected by centrifugation and washed 5 times with ethanol and dried at 60 ^oC for 24 h in vacuum environment.

2.4 Characterizations

Crystal structure was tested by the powder X-ray diffraction (XRD) patterns (Bruker D8 ADVANCE X-ray diffractometer) using Cu Kα radiation (λ=0.154178 nm with 40 kV scanning voltage, 40 mA scanning current and scanning range from 10 ° to 70°). A Hitachi S4800 type scanning electron microscopy (operated at an acceleration voltage of 3.0 kV were used to observe the size and morphology features. The sample was further characterized by the transmission electron microscope (TEM, JEM JEOL 2100). The magnetic properties were measured by a vibrating sample magnetometer (VSM, Lakeshore, Model 7400 series) at room temperature. The chemical bond was tested using a KBr pellet technique by the Fourier Transform Infrared (FT-IR, Perkin–Elmer IR spectrometer).The weight ratio was performed by inductively coupled plasma (ICP) (Optima 5300 DV). The S parameter containing S11, S12, S21 and S22 will be tested by an Agilent PNA N5224A vector network analyzer using the coaxial-line method which the samples prepared by homogeneously mixing the paraffin wax and sample (mass ratio = 1:1) and then pressing into toroidal-shaped samples (Φ_{out}:7.0 mm, Φ_{in}:3.04 mm). Then, a software which has been installed in Agilent PNA can calculate the ε', ε'', μ', μ'' values. Finally, the RL value with different thickness (*d*) can be calculated by the following formulas.[32-33]

$$Z_{in} = Z_o(\mu_r/\varepsilon_r)^{1/2}\tanh[j(2\pi fd(\mu_r\varepsilon_r)^{1/2}/c)] \quad (9)$$

$$RL(dB) = 20\log|(Z_{in}-Z_o)/(Z_{in}+Z_o)| \quad (10)$$

Where Z_{in} is the input impedance of the absorber, f is the frequency of electromagnetic wave, d is the coating thickness of the absorber while c is the velocity of electromagnetic wave in free space. ε_r ($\varepsilon_r=\varepsilon'-j\varepsilon''$) and μ_r ($\mu_r=\mu'-j\mu''$) are the complex permittivity and permeability of the absorber.

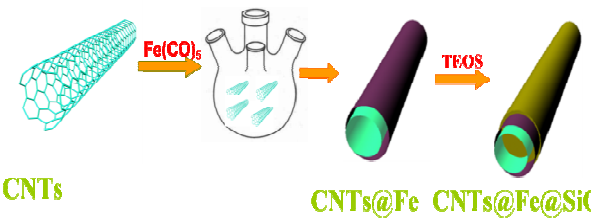

Figure 1. Synthetic scheme for the preparation of CNTs@Fe@SiO_2.

3. Results and discussion

3.1 The crystal structure, morphologies of the CNTs@Fe composite

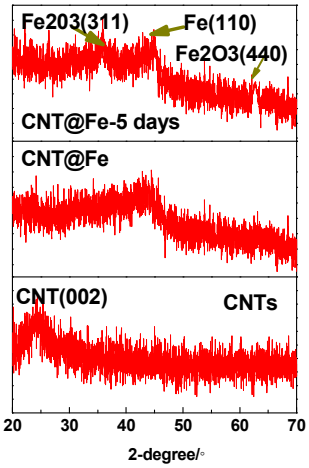

Figure 2. The XRD patterns of the CNTs and CNTs@Fe composites.

The crystal structure of the CNTs and CNTs@Fe composite was measured by XRD, as displayed in Figure 2. Pure CNTs has a broad diffraction peak at 26.4° which is assigned to (002) of CNTs. Whereas, the CNTs characteristic peak is quite weak in CNTs@Fe composite. It is noted from the CNTs@Fe sample that the diffraction peak at 44.6° is indexed to the (110) crystal plane of cubic Fe (JCPDS card No.: 06-0696). Nevertheless, the nanometer-sized Fe is not stable in air for a long time. Thus, the presence weak diffraction peaks at 35.7 and 62.7° maybe assigned to the (311) and (400) of Fe_2O_3 (JCPDS card No.: 02-1047) after exposed at air for 5 days. Just because of this, the next SiO_2 coating process is quite meaningful to avoid the Fe oxidation.

The coating thickness and morphological features of CNTs and CNTs@Fe were also determined via the SEM and TEM analysis. As can be seen from Figure 3a and 3b, CNTs have the hollow nanotube with ~40 nm out diameter and ~10 nm inner diameter. After numerous ~10 nm iron nanoparticles depositing on it (See Figure 3e), the smooth tube walls become rough (Figure 3c and d). Meanwhile, the corresponding thickness increases to 150 nm, indicating the Fe layer close to 55 nm.

In order to explore the relationship between pyrolysis time and the coating thickness, a series of time-dependent experiment were also carried out, as observed in Figure 4. It is apparent that the coating thickness is gradual increased as prolonging the decomposition time (Figure 4a-c). From Figure 3d, the diameter of CNTs@Fe is 100, 180 and 230 nm within 4, 8, and 14 h, respectively.

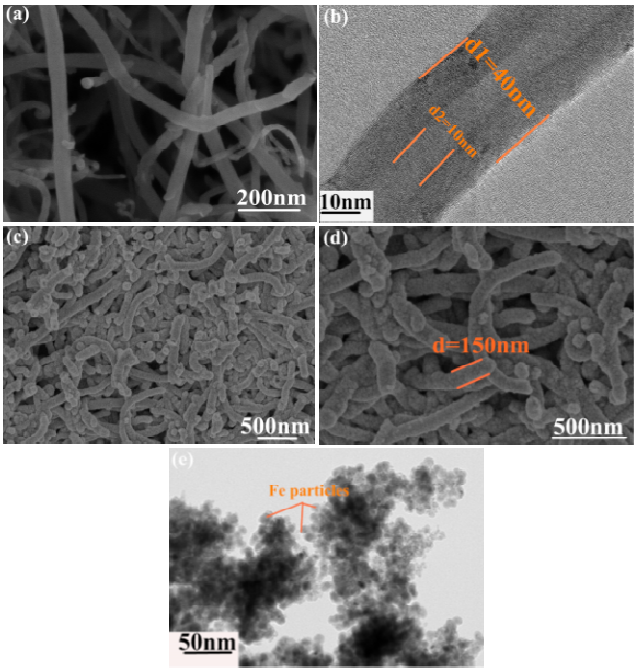

Figure 3. The SEM/TEM images: (a-b) CNTs;(c-d) CNTs@Fe composite, (e); pure Fe nanoparticles.

3.2 The crystal structure and morphologies of CNTs@Fe@SiO_2

The XRD pattern of CNTs@Fe@SiO_2 ternary composite is displayed in Figure 5. Compared with Figure 2 c and d, the new appearance of broad diffraction peak among 22-28° can be ascribed to SiO_2 coverage which is consistent with the previous result provided by Hekmatara *et al.*[34] It should be pointed out that the increase diffraction peak intensity of Fe_2O_3 is resulted from long time expose on air. Meanwhile, a tiny of Fe will be oxide during preparing SiO_2 process. However, under the SiO_2 protection, these diffraction peaks have almost no change after the sample exposed in air for 5 days.

The FT-IR spectrum was further utilized to demonstrate the presence of SiO_2 (Figure 5b). It is found that the presence of two adsorption peaks at 465 and 1091 cm^{-1}, which are associated with the Si-O-Si stretching vibration peaks of SiO_2.[35] We can also find the peak at 570 cm^{-1} in CNTs@Fe and CNTs@Fe@SiO_2 samples, which is attributed to the Fe-O bond.

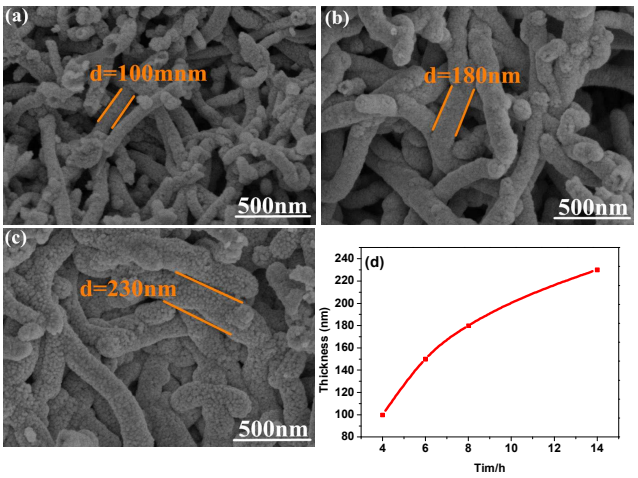

Figure 4. The SEM images of the CNTs@Fe prepared at different time (a) 4 h (b) 8 h (c)14 h. (d) is the curve of thickness vs time.

The microstructure feature of the CNTs@Fe@SiO_2 ternary composite prepared under 6 h are showed in Figure 6. As we know, the SiO_2 prepared by Stober method is easily to form nano-sphere structure. From Figure 6a, we may find that there are numerous nano-spheres with 170-200 nm in diameter. Furthermore, these nanospheres gather and assemble into necklace-like which the tube-like CNT regarded as the axis. Thus, the novel sphere-like three layers structure composed by CNTs, Fe nanoparticles as well as SiO_2 were fabricated firstly for the magnetic/dielectric core-shell electromagnetic absorbing material. The enlarged diameter also indicates that the coating thickness of SiO_2 is about 20 nm (See Figure 6b). The weight ratios of Fe, CNTs, Fe_2O_3 and SiO_2 were tested by the following steps. At the first stage, the percentage weight ratio of CNTs was tested by the HCl (0.1 M). 100 mg CNTs@Fe@SiO_2 was added into the 100 mL HCl solution and then the precipitate was collected by centrifugation. Then, the precipitate was further dissolved by the HF. Finally, the black insoluble substance was represented for the mass of CNTs. The result reveals the weight ratio of CNTs is equal to 23.1wt%. Next, the Fe element mass weight was calculated by the magnetization value of CNTs@Fe@SiO_2 (60 emu/g). It is worth mentioned that the traditional technologies including TG, ICP are hardly to test the Fe element mass ratio since the interference of Fe_2O_3 and CNTs. Whereas, the magnetization value of this composites is only come from Fe. Theoretically, the saturation magnetization value of pure Fe is equal to 218 emu/g. In the composites, the magnetization value decreases as the Fe element mass ratio decreasing. As a result, we can calculate the Fe element weight ratio is close to 27.5 wt/% (60/218=0.275). Subsequently, ICP was applied to characterized Si mass ratio. Similarity, 10 mg composite should be dissolved in a 10 mL HF solution. Then, the solution was transferred to 100 mL volumetric flaks. The ICP dates shows that Si concentration is 22.1 mg/L. Thus, the SiO_2 weight ratio is 45.2 wt%. Finally, the mass weight of Fe_2O_3 is 4.2 wt%. Actually, the influence of Fe_2O_3 in the finally electromagnetic absorption can be ignored with the following reason: The electromagnetic parameters of Fe_2O_3 (ε'=3-4, ε''=0) are almost equal to the SiO_2, which is good for the impedance matching behavior and weak at attenuation. As a result, Fe_2O_3 has no contribution to the attenuation of electromagnetic wave.

3.3 Magnetic and electromagnetic absorption properties of the samples

The magnetic properties of the CNTs@Fe and CNTs@Fe@SiO_2 composites were tested by a vibrating sample magnetometer. Obviously, the magnetization values are mainly originated from the presence of Fe in these two samples. The CNTs@Fe shows a high magnetization value of 103 emu/g, higher than CNTs@Fe@SiO_2 (60 emu/g). However, for many magnetic/dielectric materials, their magnetization values are no more than 50 emu/g due to the lower saturation magnetization.

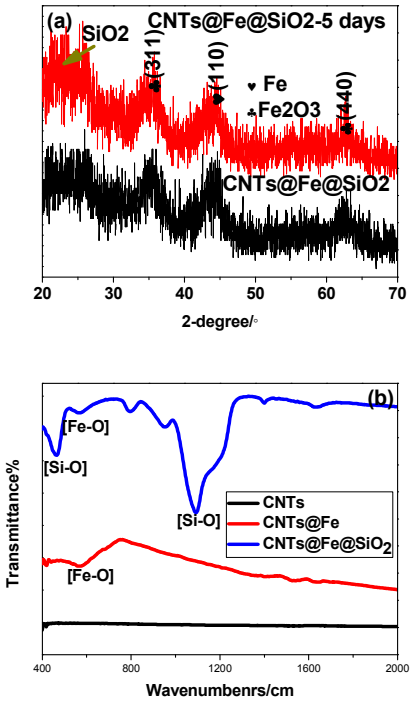

Figure 5. The XRD patterns (a) and FT-IR diagram (b) of CNTs, CNTs@Fe and CNTs@Fe@SiO_2.

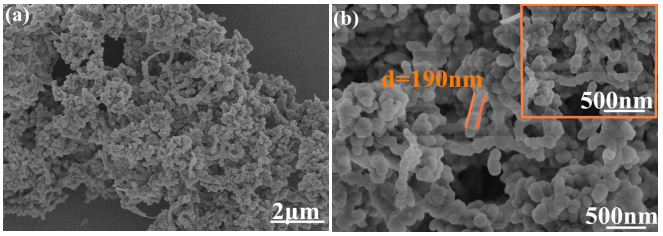

Figure 6. The SEM images of the CNTs@Fe@SiO_2 composite.

The calculated reflection loss data was displayed in Figure 8.An excellent electromagnetic absorption material should have a lower reflection loss value, broad effectively frequency range and lightweight. In generally, the reflection loss value less than -10 dB (corresponding to less than 10 % of reflection, named RL_{min}) are as broader as possible. In order

to satisfy the lightweight, the coating thickness (t) is not too thickness (in practical application, t <2 mm). It is easily to find that the RL_{min} value of pure CNTs at all thickness (1.5-3.5 mm) is even not exceeding -6 dB, which indicates that the pure CNTs are not a good candidate for practical use (see Fig. 8a). Clearly, after coating Fe, RL_{min} exhibits an obvious improvement (Figure 8b). The minimum reflection loss value of -12.8 dB is obtained with a thin coating thickness of 1.5 mm. At the same time, the peak shifts to lower frequency region as increasing the coating thickness. That can be explained by the 1/4 wavelength equation:[36-37]

$$t_m = nc/4f_m(\varepsilon_r \mu_r)^{1/2} \quad (11)$$

Where t_m and f_m represent for the matching thickness and frequency of the RL_{min} peaks, C is the velocity of light. As far as the CNTs@Fe@SiO_2 is concerned, the RL_{min} value increases to -14.2 dB at the identical 1.5 mm which is much higher than most of other reported dielectric/magnetic composites, including Ni@CuO (-11 dB)[38], Co/CoO(-14 dB)[39], Fe@SnO_2(-10.1dB)[40],Fe_3O_4@$CuSiO_3$ (<-10 dB)[41-42] and Fe_3O_4@ZrO_2[43] (<-10 dB). In addition, the reflection loss for the ternary composite also shows the remarkable advantage at other coating thickness. For example, the RL_{min} value of CNTs@Fe@SiO_2 reaches to -22.3 dB while the CNTs@Fe is only -11.1 dB with the identical 3 mm thickness. The effective frequency is another important factor to evaluate the electromagnetic absorption, as described in Figure 8d-f. The yellow and green areas stand the effective frequency region. From Figure 8d, one can find that the pure CNTs have no yellow area. The as-prepared CNTs@Fe composite has three small areas which located in 3.8-3.2, 4.6-4.9, 10.5-12.5 GHz with the corresponding thickness of 3.45-3.5, 2.95-3.05 and 1.5-1.7 mm, respectively (Figure 8e). The CNTs@Fe@SiO_2 ternary composite exhibits the largest effectively frequency region. In detail, the corresponding frequency region locates in 5.9-15.7 and 16.9-18 GHz with the thickness of 1.8-3.5 and 1.5-1.7 mm.

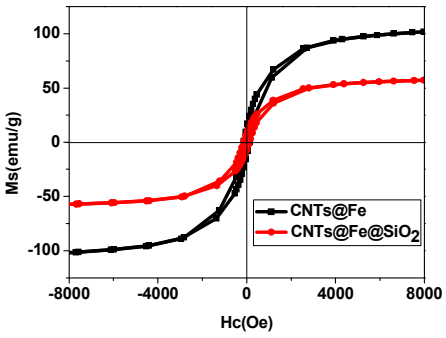

Figure 7. The M-H loop of the CNTs@Fe and CNTs@Fe@SiO_2 composites.

In order to analyze the difference in electromagnetic absorption properties, the corresponding electromagnetic parameters have been illustrated in Figure 9. In electromagnetic absorption field, the real and imaginary parts of permittivity are representing for the storage and loss ability for electromagnetic wave, respectively. As can be seen from Figure 9a, both Fe and SiO_2 coating layer do contribution to the ε'. For the pure CNTs, ε' is among 90-100. But, the larger ε' presents obviously decrease tendency since Fe and SiO_2 layer introducing. Such a decrease is beneficial for electromagnetic absorption. The ε' value of CNTs@Fe is only among 20-30 while the CNTs@Fe@SiO_2 remains the smallest value of 12-10. As far as the imaginary part of permittivity value is concerned, the three samples share the same tendency which the values are ranged in the following order: CNTs>CNTs@Fe>CNTs@Fe@SiO_2. It is worth noted that a high ε'' value will result in a strong attenuation wave ability. Although the CNTs@Fe@SiO_2 shows the lowest ε'' value of 3-5, it is still bigger than most of pure magnetic materials such as the hollow-like Fe_3O_4 (0-2)[44], hexagonal-like FeCo (1-2.8)[45], coin-like Fe (0-2)[46].

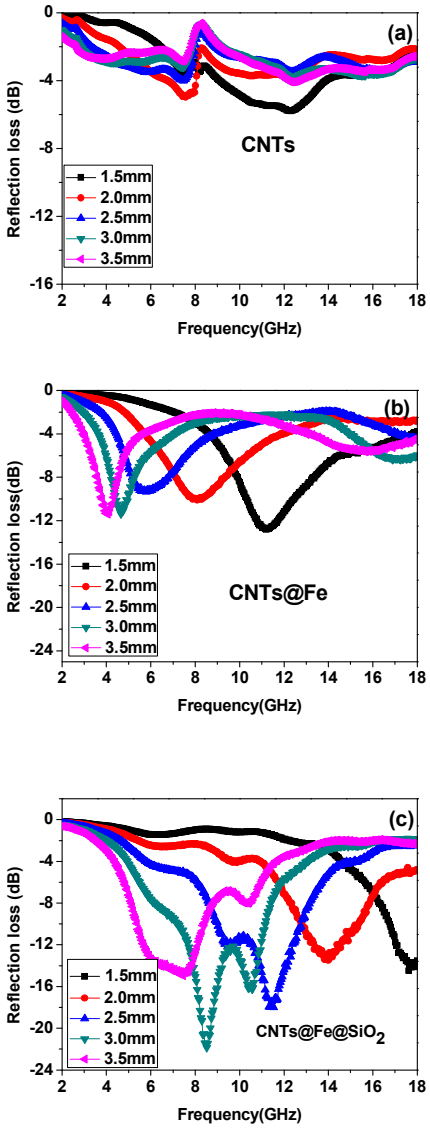

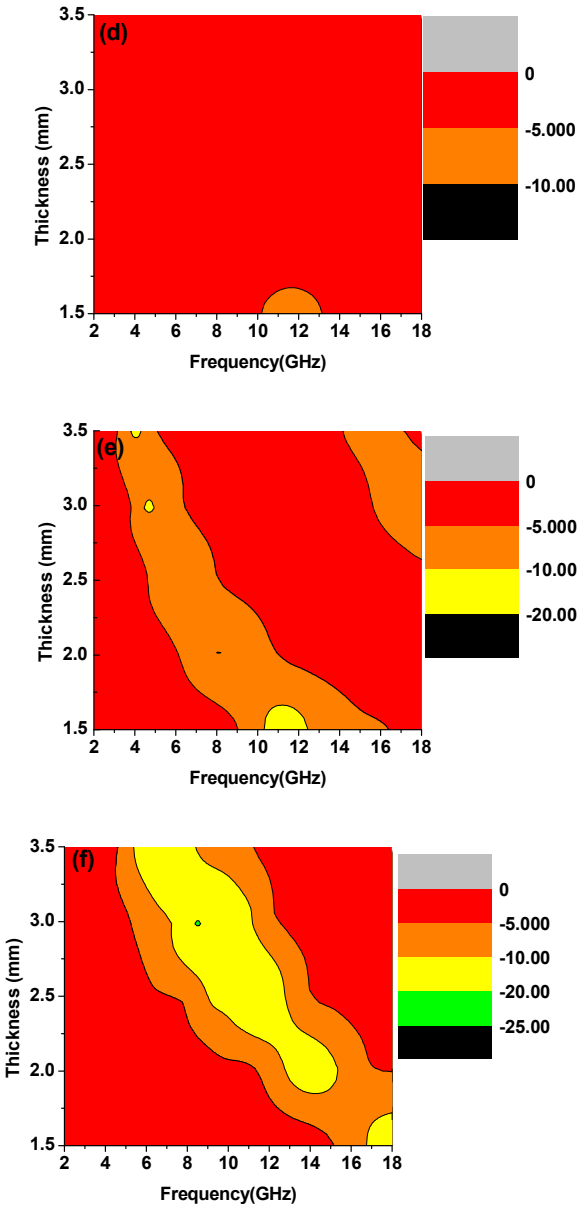

Figure 8. The RL dates and effective frequency regions (a) (e): CNTs; (b) (e): CNTs@Fe; (c) (f) CNTs@Fe@SiO_2.

Nevertheless, it is difficult to judge the electromagnetic absorption properties just relying on the electromagnetic parameters. In fact, the enhanced electromagnetic absorption properties may directly attribute to the impedance matching properties and attenuation constant α, which are calculated by the following equation:[47]

$$\alpha=\frac{\sqrt{2}\pi f}{c}\times\sqrt{(\mu\varepsilon''-\mu\varepsilon')+\sqrt{(\mu\varepsilon''-\mu\varepsilon')^2+(\mu\varepsilon'+\mu\varepsilon')^2}} \quad (12)$$

The attenuation constant α symbolizes the integral attenuation ability. In other words, a strong magnetic loss and dielectric loss may lead to increase the attenuation constant α, but a high α value not means a strong dielectric or magnetic loss ability. Different from the attenuation constant α, the impedance matching value directly reveals the interface reflection properties, as shown in Figure 10a. The pure CNTs show the poor impedance matching value. This is the main reason why the high ε'' of CNTs is still hardly to obtain an ideal electromagnetic absorption property. After the Fe coating, the impedance matching ratio has significantly improved. Figure 10a also indicates that the impedance matching ratio of CNTs@Fe further increase since modified by SiO_2 coating layer. From Figure 10b, the CNTs@Fe exhibits the highest attenuation constant α while the pure CNTs is lowest.

As a result, we can get information that the CNTs@Fe@SiO_2 with the optimal electromagnetic absorption may be originated from the factors, as depicted in Figure 11. At the first stage, the high impedance matching property is able to make most of the electromagnetic wave incidence into the coating layer. Then, the multi-interface polarization effects, in particular the Fe-C polarization, play a vital role on the electromagnetic wave attenuation. It is well-known that the hexagonal crystal structure of carbon with sp^2 hybrid exhibits many free electrons[48]. After the Fe coating over the carbon, the Fe atom is easily induced by these free electrons which may form momentary separation of Fe atomic nucleus and extranuclear electrons (Fe atom = Fe atomic nucleus+extranuclear electrons). The generated electrons by Fe may be further spread among the Fe atom and then induce outer layer of Fe polarization. Such polarization and electron transmission procedure is dynamic and needs the electromagnetic wave provide energy. But, the electromagnetic wave incidence the surface carbon, the high electrical conductivity of carbon enables the electromagnetic wave transfer in the form of microcurrent. A small part of electromagnetic wave maybe attenuates during the transmission process. The SiO_2 wave-transparent layer should not be ignored. One the one hand, the presence the SiO_2 coating layer will let more and more electromagnetic wave incidence into the Fe layer and CNTs. One the other hand, without the protection of SiO_2, the Fe layer will be oxidized deeply after exposed in air. If Fe exhibits in the form of Fe^{3+} or Fe^{2+}, the interface polarization between Fe-C may obviously decrease, which is bad for electromagnetic wave attenuation. The SiO_2 coating layer also contributes to suppress the eddy current loss of Fe layer.

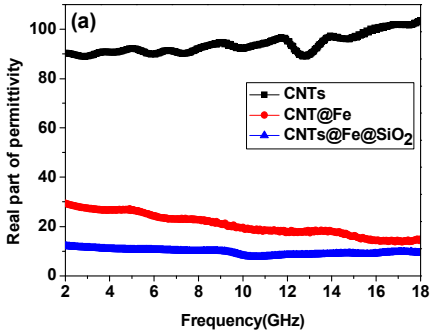

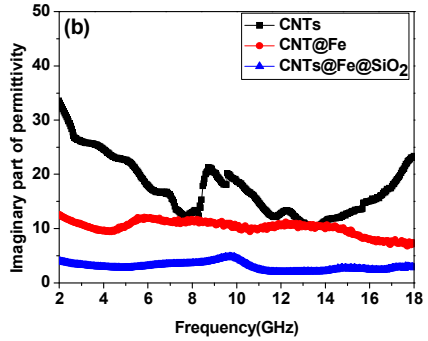

Figure 9. The real (a) and imaginary part (b) of permittivity of three samples.

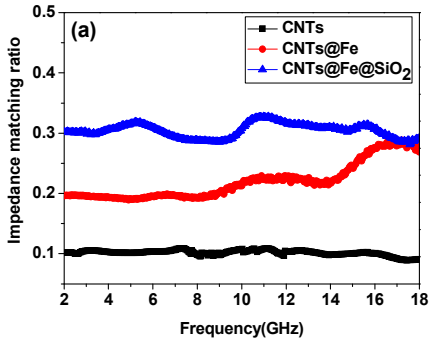

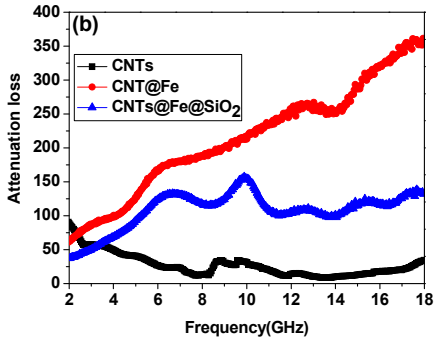

Figure 10. The impedance matching (a) and attenuation loss α (b).

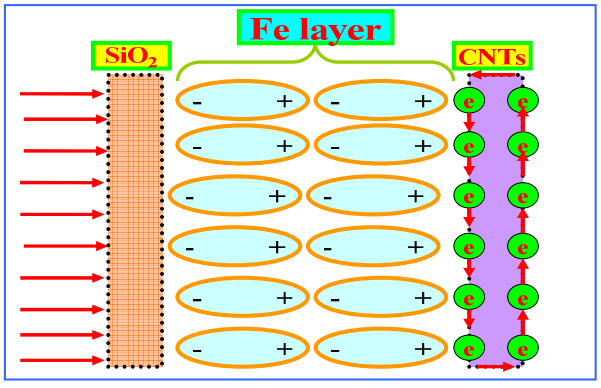

Figure 11. The possible electromagnetic wave attenuation mechanism.

4. Conclusion

In summary, the CNTs@Fe@SiO_2 composite has been synthesized by a two-step method which the Fe was generated by the $Fe(CO)_5$ decomposition approach. Then, the Stober method was applied to coat SiO_2 onto the CNT@Fe. Such a ternary composite presents an excellent electromagnetic absorption performance at a thin thickness. An optimal reflection loss value of -14.2 dB was obtained at only 1.5 mm, which great meets the demands of light-weight. The possible absorption mechanism also has been discussed in this study.

Corresponding Author

* E-mail: gbji@nuaa.edu.cn

Acknowledgments

Financial support from the Aeronautics Science Foundation of China (no. 2014ZF52072), the National Natural Science Foundation of China (no. 51172109 and 11475086), the Fundamental Research Funds for the Central University (no. 3082014NS2014057), and the Priority Academic Program Development of Jiangsu Higher Education Institutions is gratefully acknowledged. This work also support from the Funding for Outstanding Doctoral Dissertation in NUAA(BCXJ15-09).

Notes and references

[a] *College of Materials Science and Technology, Nanjing University of Aeronautics and Astronautics, Nanjing 211100, P. R. China.*
[b] *National Laboratory of Solid State Microstructures, Nanjing University, Nanjing 210093, P. R. China.*

1 J.Rouhi, C.H. Raymond Ooi, S. Mahmudd, M. R. Mahmood, *Mater. Lett.*, 2015, **147**, 34–37.
2 R.C. Jin, Y.S. Guan, H. Liu, J.H. Zhou, G. Chen, *ChemPlusChem* 2014, **79**, 1643-1648.
3 4 T. Liu, Y. Pang, M. Zhu, S. Kobayashib, *Nanoscale*, 2014, 6, 2447-2454.
4 M.K.Han, X.W.Yin, L.Kong, M.Li, W.Y.Duan, L.T.Zhang, L.F.Cheng, *J.Chem.Mater.A*, 2014, **2**,16403-16409.
5 D.P. Sun, Q. Zou, Y.P. Wang, Y.J. Wang, W. Jiang, F.S. Li, *Nanoscale*, 2014, **6**, 6557-6562.
6 X.H. Li, J. Feng, H. Zhu, C.H. Qu, J.T. Bai, X.L. Zheng, *RSC Adv.*, 2014, **4**, 33619-33625.
7 H.L. Lv, G.B. Ji, M. Wang, C.M. Shang, H.Q. Zhang, Y.W. Du, *RSC Adv.*, 2014, 4, 57529-57533.
8 Z.X. Yu, Z.P. Yao, N. Zhang, Z.J. Wang, C.X. Li, X.J. Han, X.H. Wu, Z.H. Jiang, *J. Mater. Chem. A*, 2013, **1**, 4571-4576.
9 W.C. Zhou, X.J. Hu, X.X. Bai, S.Y. Zhou, C.H. Sun, J. Yan, P. Chen, *ACS Appl. Mater. Interfaces,* 2011, **3**, 3839-3845.
10 L. Wang, Y. Huang, C. Li, J.J. Chen, X. Sun, *Phys. Chem. Chem. Phys,* 2015,**17**, 5878-5886.
11 J.W. Liu, J. Cheng, R.C Che, J.J. Xu, M.M. Liu, Z.W. Liu, *J. Phys. Chem.* C 2013, 117, 489-495.
12 J.W. Liu, J.J. Xu, R.C. Che, H.J. Chen, M.M. Liu, Z.W. Liu, *Chem. Eur. J.* 2013, **19**, 6746-6752.
13 C.L. Zhu, M.L. Zhang, Y.J. Qiao, G. Xiao, F. Zhang, Y.J. Chen, *J. Phys. Chem. C* 2010**, 114**, 16229-16235.
14 Z.J. Wang, L. Wu, J.G. Zhou, B.Z. Shen, Z.H. Jiang, *RSC Adv.*, 2013, **3**, 3309-3315.

15 Y.C. Du, W.W Liu, R. Qiang, Y. Wang, X.J. Han, J. Ma, P. Xu, *ACS Appl. Mater. Interfaces,* 2014, **6**, 12997-13006.
16 B. Zhao, G. Shao, B.B. Fan, W.Y. Zhao, R. Zhang, *RSC Adv.*, 2014, **4**, 57424-57429.
17 B. Zhao, G. Shao, B.B. Fan, W.Y. Zhao, Y.J. Xie, R. Zhang, *RSC Adv.*, 2014, **4**, 61219-61225.
18 G.Z. Wang, X.G. Peng, L. Yu, G.P. Wan, S.W. Lin, Y. Qin, *J. Mater. Chem. A*, 2015, **3**, 2734-2740.
19 J. J. Jiang, X. J. Li, Z. Han, D. Li, Z. H. Wang, D. Y. Geng, S. Ma, W. Liu, Z. D. Zhang, *J. Appl. Phys.* 2014, **115**, 17A514-17A516.
20 T. Wei, C. Q. Jin, W. Zhong, J. M. Liu, 2007, **91**, 222907-222909.
21 L. Kong, X.W Yin, F. Ye, Q. Li, L.T. Zhang, L.F. Cheng, *J. Phys. Chem. C,* 2013, 117, 2135-2146.
22 C.K. Cui, Y.C. Du, T.H. Li, X.Y. Zheng, X.H. Wang, X.J. Han, P. Xu, *J. Phys. Chem. B*, 2012, **116**, 9523-9531.
23 Q.M. Su, J. Li, G. Zhong, G.H. Du, B.S. Xu, *J. Phys. Chem. C,* 2011, **115**, 1838-1842.
24 J. Qiu, T.T. Qiu, *Carbon*, 2015, **81**, 20-28.
25 C.L. Zhu, M.L.Zhang, Y.J. Qiao, G. Xiao, F. Zhang, Y.J. Chen, *J. Phys. Chem. C*. 2010, **114**, 6229-6235.
26 W.L. Zuo, L. Qiao, X. Chi, T. Wang, F.S. Li, *J. Alloys, Compds,* 2011, **509**, 6359-6363.
27 T. Liu, P. H. Zhou, J. L. Xie, and L. J. Deng, *J. Appl. Phys*, 2012, **111**, 093905-09309.
28 W.W. Liu, H. Li, Q.P. Zeng, H.N. Duan, Y.P. Guo, X.F. Liu, C.Y. Sun, H.Z Liu, *J. Mater. Chem. A,* 2015,**3**, 3739-3747.
29 Y. Liu,X.X. Liu , R. Li, W. Wen, X.J. Wang, *RSC Adv.*,2015, **5**, 8713-8720.
30 Z.H. Yang, Z.W. Li, L.H. Yu, Y.H.Yang, Z.C. Xu, *J. Mater. Chem. C*, 2014, 2, 7583-7588.
31 R. D. Desautels, M.P. Rowe, M. Jones, A. Whallen, J.V. Lierop, *Langmuir*, 2015, **31**, 2879-2884.
32 Z.T. Zhu, X. Sun, H.R. Xue, H. Guo, X.L. Fan, X.C. Pan, J.P. He, *J. Mater. Chem. C*, 2014, **2**, 6582-6591.
33 X. Jian, X.G. Chen, Z.W. Zhou, G. Li, M. Jiang, X.L. Xu, J. Lu, Q.M. Li, Y.Wang, J.H. Goue, D. Hui, *Phys. Chem. Chem. Phys.,* 2015, **17**, 3024-3031.
34 H. Hekmatara, M. Seifi, K. Forooraghi, S. Mirzaee, *Phys. Chem. Chem. Phys.,* 2014, 16, 24069-24075.
35 J. Wang, W. Zhu, L.X. Liu, Y.M. Chen, C. Wang, *ACS Appl. Mater. Interfaces*, 2015, **9**, 5454-5461.
36 G. M. Li, L. C. Wang, W. X. Li, R. M. Ding and Y. Xu, Phys. *Chem. Chem. Phys.*, 2014, **16**, 12385-12392.
37 H.L. Lv, X.H. Liang, Y. Cheng, H.Q. Zhang, D.M. Tang, B.S. Zhang, G.B.Ji,Y.W. Du, *ACS Appl. Mater. Interfaces*, 2015, **7**, 4744-4750.
38 B. Zhao, G. Shao, B.B. Fan, W.Y. Zhao, R. Zhang, *Phys. Chem. Chem. Phys.,* 2015, **17**, 6044-6052.
39 Z.Z. Wang, H. Bi, P.H. Wang, M. Wang, Z.W. Liu, L. shen, X.S. Liu, *Phys. Chem. Chem. Phys.,* 2015, **17**, 3796-3801.
40 X.G. Liu,G.P. Zhou, S. Wing , Y.P. Sun, *RSC Adv.*, 2014, **4**, 51389-51394.
41 J.J. Xu, J.W. Liu, R.C. Che, C.Y. Liang, M.S. Cao, Y. Li, Z.W. Liu, *Nanoscale*, 2014, **6**, 5782-5790.
42 J.W. Liu, J. Cheng, R.C. Che, J.J. Xu, M.M. Liu, Z.W. Liu, *ACS Appl. Mater. Interfaces,* 2013, **5**, 2503-2509.
43 M. Yu, C.Y. Liang, M.M. Liu, X.L. Liu, K.P. Yuan, H. Cao, R.C. Che, *J. Mater. Chem. C*, 2014, **2**, 7275-7283.
44 Y. Yang , Y. Yang, X. Wen, J. Ding, J. *Appl. Phys*., 2014, **115**, 17A521-17A523.
45 H.L. Lv, G.B. Ji, M. Wang, C.M. Shang, H.Q. Zhang, Y.W. Du, *J. Alloys, Compds*, 2014, **615**,1037-1042.
46 H.L. Lv, X.H. Liang, Y. Cheng, G.B. Ji, D.M. Tang, B.S. Zhang, H.Q. Zhang, Y.W. Du, *RSC Adv.*, 2015, **5**, 25936–25941.
47 K. S. Novoselov, A. K. Geim, S. V. Morozov, D. Jiang,Y. Zhang, S. V. Dubonos, I. V. Grigorieva, A. Fiesov,*Science*, 2004, **306**, 666-670.
48 S.L. Zhang, Q.Z. Jiao, Y. Zhao, H.S. Li, Q. Wu, *J.Mater. Chem.A,* 2014, **2**, 18033-18039.